Published in final edited form as:

Cancer Res. 2021 May 01; 81(9): 2415–2428. doi:10.1158/0008-5472.CAN-20-2705.

Host-derived Matrix Metalloproteinase-13 Activity Promotes Multiple Myeloma-induced Osteolysis and Reduces Overall Survival

Chen Hao Lo[1,2,*], **Gemma Shay**[1,*], **Jeremy J McGuire**[1], **Tao Li**[1], **Kenneth Shain**[3], **Jun Yong Choi**[4], **Rita Fuerst**[5], **William R Roush**[6], **Anna M Knapinska**[7], **Gregg B Fields**[8], **Conor C Lynch**[1,†]

[1]Department of Tumor Biology, H. Lee Moffitt Cancer Center, Tampa, FL, 33612.

[2]Cancer Biology Ph.D. Program, Department of Cell Biology Microbiology and Molecular Biology, University of South Florida, Tampa, FL, 33612.

[3]Department of Malignant Hematology, H. Lee Moffitt Cancer Center, Tampa, FL, 33612.

[4]Department of Chemistry and Biochemistry Queens College, Queens, NY 11367, and Ph.D. Programs in Chemistry and Biochemistry, The Graduate Center of the City University of New York, New York, NY 10016

[5]Department of Organic Chemistry, Graz University of Technology, 8010 Graz, Austria

[6]Department of Chemistry, Scripps Research Institute, Jupiter FL 33458

[7]Alphazyme, LLC, 225 Chimney Corner Ln Suite 3021, Jupiter, FL 33458 ania.knapinska@alpha-zyme.com

[8]Institute for Human Health & Disease Intervention (I-HEALTH) and Department of Chemistry & Biochemistry, Florida Atlantic University, Jupiter, FL 33458.

Abstract

Multiple myeloma promotes systemic skeletal bone disease that greatly contributes to patient morbidity. Resorption of type-I-collagen rich bone matrix by activated osteoclasts (OCL) results in the release of sequestered growth factors that can drive progression of the disease. Matrix metalloproteinase-13 (MMP-13) is a collagenase expressed predominantly in the skeleton by mesenchymal stromal cells (MSC) and MSC-derived osteoblasts. Histochemical analysis of human multiple myeloma specimens also demonstrated that MMP-13 largely localizes to the

[†]**Corresponding Author:** Conor C. Lynch, Tumor Biology Department, SRB-3, H. Lee Moffitt Cancer Center & Research Institute, 12902 Magnolia Drive, Tampa, FL, 33612. Tel: +1-813-745-8094, conor.lynch@moffitt.org.

Author contributions: C. H. Lo, G. Shay and C. C. Lynch were responsible for study conception and design. C. H. Lo, G. Shay, J. J. McGuire and C. C. Lynch developed the methodology. J. Y. Choi, R. Fuerst and W. R. Roush generated the MMP-13i reagents; A. Knapinska and G. B. Fields generated biochemical data for and biologically characterized the MMP-13i reagents. C. H. Lo, G. Shay, J. J. McGuire and T. Li acquired the data while C. H. Lo, G. Shay, K. Shain and C. C. Lynch were responsible for analysis and interpretation of data. C. H. Lo, G. Shay and C. C. Lynch were responsible for manuscript writing. C. H. Lo, G. Shay, J. J. McGuire, T. Li, J. Y. Choi, R. Fuerst, W. R. Roush, A. Knapinska, G. B. Fields, K. Shain and C. C. Lynch reviewed the manuscript.

[*]Both authors contributed equally to this work

Disclosures of Potential Conflicts of Interest: A. M. Knapinska is President and CEO of MMP Biopharma. G. B. Fields is Vice-President of MMP Biopharma. The other authors have no potential conflicts of interest to disclose.

stromal compartment compared to CD138+ myeloma cells. In this study, we further identified that multiple myeloma induces MMP-13 expression in bone stromal cells. Because of its ability to degrade type-I-collagen, we examined whether bone stromal derived MMP-13 contributed to myeloma progression. Multiple myeloma cells were inoculated into wild type or MMP-13 null-mice. In independent in vivo studies, MMP-13 null mice demonstrated significantly higher overall survival rates and lower levels of bone destruction compared to wild type controls. Unexpectedly, no differences in type-I-collagen processing between the groups were observed. Ex vivo stromal co-culture assays showed reduced formation and activity in MMP-13-null osteoclasts. Analysis of soluble factors from wild type and MMP-13-null MSCs revealed decreased bioavailability of various osteoclastogenic factors including CXCL7. CXCL7 was identified as a novel MMP-13 substrate and regulator of osteoclastogenesis. Underscoring the importance of host MMP-13 catalytic activity in multiple myeloma progression, we demonstrate the in vivo efficacy of a novel and highly-selective MMP-13 inhibitor that provides a translational opportunity for the treatment of this incurable disease.

Keywords

Multiple Myeloma; MMP-13; MSC; Osteoclasts; CXCL7

Introduction

Multiple myeloma is an incurable plasma cell malignancy that colonizes the skeleton. Osteoclast-mediated bone destruction is a major hallmark of active disease. The resultant lesions cause great pain, contributing to patient morbidity and mortality. Interaction with the bone stroma can protect multiple myeloma cells from applied therapies, and the associated degradation of bone matrix generates growth factors that further drive the progression of the disease[1]. Agents such as bisphosphonates and receptor activator of nuclear kappa B ligand (RANKL) inhibitors effectively reduce osteoclast numbers and protect against skeletal-related disease but offers little benefit in regards to overall survival[2]. These data suggest additional mechanisms facilitate myeloma-bone interaction and their identification could yield novel therapeutic targets for the treatment of the disease.

Mineralized bone matrix is primarily resorbed by osteoclasts. Over 90% of bone is comprised of mineralized type I collagen and therefore enzymes with collagenolytic activity are crucial for appropriate bone remodeling. Cathepsin K is an acidophilic collagenase suited to working in the low pH of the osteoclast lacunae[3–5]. However, collagenolytic MMPs, namely MMP-1, -2, -8, -13 and membrane-bound MMP-14, -15 are expressed in bone and ablation of these MMPs in mice has demonstrated skeletal phenotypes in particular for MMP-14[6–11]. These phenotypes can be attributed to extracellular matrix (ECM) turnover and the processing of non-matrix molecules such as growth factors and cytokines. Counterintuitively, MSCs and osteoblasts that are responsible for bone matrix deposition express the majority of these MMPs compared to osteoclasts[12–14]. MMPs are also secreted by myeloma cells[15, 16]. Interestingly, recent studies have reported a non-catalytic role for myeloma-derived MMP-13 in disease progression[17], but the catalytic role for stroma-derived MMP-13 remains unexplored. Here, our analyses of human

myeloma biopsies demonstrate MMP-13 expression in bone-lining osteoblasts and MSCs. This is consistent with literature showing widespread MMP-13 expression in the skeleton by cells of mesenchymal stromal cell (MSC) lineage, including chondrocytes, osteoblasts and osteocytes[18–20]. Additionally, MMP-13 appears not to be expressed by osteoclasts although reports have localized MMP-13 in peri-osteoclast cells and in the cement lines of the bone matrix[19, 21].

To date, no studies have examined the contribution of host-derived MMP-13 on myeloma progression. This is in large part due to the paucity of myeloma models that allow for the ablation of host-derived genes of interest. The spontaneously arising murine myeloma cell line 5TGM1 is syngeneic to the KaLwRiJ sub-strain of C57BL/6. The cells do not grow in C57BL/6 mice, but we have previously reported that 5TGM1 engraftment in C57BL/6 recombinase activating gene-2 (RAG-2)-null mice is feasible[22, 23]. We therefore generated novel RAG-2- and MMP-13-double null C57BL/6 mice that would allow us to address the contribution of host-derived MMP-13 to the progression of multiple myeloma. Our findings show that host compartment MMP-13 ablation significantly improved the overall survival of myeloma-bearing mice as a result of decreased bone resorption. Surprisingly, this was not due a deficiency in type I collagen turnover but rather differences in the bioavailability of factors, namely CXCL7, that promote osteoclast precursor recruitment and formation. To determine the translatability of MMP-13 inhibition as a therapeutic approach, we also demonstrate the efficacy of a highly-selective MMP-13 inhibitor using an immunocompetent *in vivo* model. Taken together, our data identify, for the first time, a causal role for host-derived MMP-13 catalytic activity in driving the progression of multiple myeloma.

Materials and Methods

Human patient specimens, MMP-13-null mice, multiple myeloma cell lines, and MMP-13 inhibitors

Deidentified human patient specimens were collected through Moffitt Cancer Center's Institutional Review Board-approved Total Cancer Care protocol (MCC14690). All patients involved in this study provided written informed consent in accordance with recognized ethical guidelines as detailed in the Belmont Report. Animal experiments were performed under the University of South Florida-approved Institutional Animal Care and Use Committee (IACUC) protocol, IS0000309, IS0003489 and IS0005900. RAG-2/MMP-13 double-null mice were generated by crossing RAG-2-null mice with MMP-13-null mice, on a C57BL/6 background. Luciferase-labeled myeloma cells, 5TGM1-Luc (RRID:CVCL_VI66) and U266-Luc (RRID:CVCL_0566) were obtained from University of Texas, Health Science Center at San Antonio, TX (2012) [24] and University of Virginia, VA (2014), respectively. MM1.S were obtained in 2015 from ATCC (Cat#: CRL-2974; RRID:CVCL_8792) and OPM2 was obtained in 2015 from Dr. Kenneth Shain (Moffitt Cancer Center; RRID:CVCL_1625). Cells were cultured in RPMI containing 10% FBS, 1% penicillin and streptomycin, used within 30 passages. Cells have recently tested negative for mycoplasma by PCR in July 2020 (Bulldog Bio, Cat #: 25233), and were additionally authenticated against ATCC, DSMZ or ExPASy STR profiles. Compound 1 ((*S*)-**17b** in

reference 25), Compound 2 ((*S*)-**17c** in reference 25) and Compound 4 (**52** in reference 26) were synthesized as described in the respective references[25, 26]. For the majority of the studies, unless otherwise explicitly stated, we used Compound 1 as the MMP-13 inhibitor and denoted it as MMP-13i.

Bioinformatics analysis of NCBI GEO and MMRF human datasets

NCBI dataset GSE47552 consists of RNA sequencing data from CD138+ cells isolated from healthy donors and MGUS, SMM and MM patients (n=99). *MMP-1*, *MMP-8* and *MMP-13* expressions was extracted and analyzed using the web built-in GEO2R software per NCBI instructions. NCBI dataset GSE46053 consists of transcriptomic sequencing data from healthy donor- and myeloma patient-derived MSCs which were or were not conditioned using human myeloma (MM1.S) conditioned media (n=37). Myeloma-induced *MMP-1*, *MMP-8* and *MMP-13* expressions were extracted and analyzed using the web built-in GEO2R software per NCBI instructions. Multiple Myeloma Research Foundation (MMRF) IA14 is a record repository for the CoMMpass study, which tracks genomic status throughout myeloma disease progression in newly-diagnosed treatment-naïve patients. Analyses of 770 enrolled individuals with RNA sequencing data paired with their longitudinal clinical data was performed using built-in analytical tools online to compare gene expression with progression free survival and overall survival.

Immunohistochemical (IHC) and immunofluorescence (IF) staining

Non-sequential FFPE, rehydrated tissue sections were rinsed with 1XTBST. Endogenous peroxidases were quenched using methanol peroxide. Antigen retrieval was performed using proteinase K (20μg/ml) at 25°C for 10 minutes. 4% paraformaldehyde-fixed *in vitro* chamber slides proceeded directly with the following. Cells and tissues were blocked at 25°C for one hour, and incubated overnight at 4°C in primary antibody diluted in blocking reagent: α-human/mouse MMP-13 at 1:200 (Triple Point Biologics, Cat#: RP1-MMP-13), α-human CD138 at 1:200 (BD Pharmingen, Cat#: 553712; RRID:AB_394998), and α-mouse IgG2b (Bethyl Laboratories, Cat#: A90–109A; RRID:AB_67157 at 1:200 and A90–109P; RRID:AB_67160 at 1:1000 for immunofluorescence and western blot, respectively). Isotype controls were used to assess antibody specificity. Sections were then washed in 1XTBST, and incubated either with species-specific biotinylated or fluorescently-labeled (Invitrogen) secondary antibodies at 1:1000 in blocking buffer for 1 hour at 25°C for IHC and IF staining, respectively. For IHC, biotinylated targets were visualized after 1XTBST washes using an avidin-biotin peroxidase complex and DAB. Sections were counterstained with hematoxylin, dehydrated and mounted for brightfield microscopy. For IF studies, stained slides were counterstained with DAPI and aqueously mounted for wide-field fluorescence microscopy.

Mesenchymal stromal cell and osteoclast precursor isolation and differentiation.

Mesenchymal stromal cells (MSC) were isolated from both male and female bone marrow flushes and fragmented bone chips harvested from neonatal RAG-2-null/ wild-type and MMP-13-null mice[27, 28]. Tissues were digested in MSC medium (α-MEM containing 15% FBS) and 1mg/mL collagenase for 1 hour at 37°C with shaking at 150rpm and were

cultured in MSC medium for 3 days. Adherent populations were enriched by carefully removing non-adherent cells over time. MSCs were validated in osteogenic assays and expanded for further analysis.

Murine femoral and tibial bone marrow were plated in 10cm petri dishes in 10mL α-MEM medium containing 10% FBS to generate primary osteoclasts *in vitro*. Non-adherent population was re-plated in fresh dishes with media containing 25 ng/ml of M-CSF (Peprotech, Cat#: 315-02-10) to enrich for myeloid osteoclast precursor population. Myeloid progenitors were subsequently plated at $2–3\times10^5$ /well in 48- or 96-well cell culture plates and treated every 48 hours with osteoclastogenic medium: α-MEM containing 10% FBS, 25ng/ml M-CSF, and 100ng/ml RANKL (Peprotech, Cat#: 315-11-10) for 4 to 7 days. For treatment studies, MMP-13i (Compound 1) was added to osteoclastogenic media (10nM-10μM) to assess its effect on differentiation. For MSC conditioned media studies on osteoclast formation, control and CXCL7-immunoprecipitated MSC conditioned media (24-hours in α-MEM with 15% FBS) was collected from wild-type and MMP-13-null MSCs and used at 1:1 ratio with regular osteoclast media supplemented with RANKL but without MCSF. For treatment studies with recombinant CXCL7 protein, precursor cells were periodically fed with differentiation media containing full-length or MMP-13-processed recombinant CXCL7 (Beta Lifesciences, Cat#: BL-0262PS) for up to 5 days. Differentiated cultures were fixed in 4% paraformaldehyde and stored at 4°C in 1XPBS.

In vitro osteoclast tartrate-resistant acid phosphatase (TRAcP) staining, resorption assay and osteoblast differentiation and alizarin red staining

TRAcP was performed on fixed *in vitro* differentiated osteoclasts co-cultures to detect multinucleated osteoclasts using Histostain-TRAcP Kit per manufacturer's instructions (Invitrogen, Cat#: 85–0199). For *in vitro* resorption assays, bone marrow myeloid precursor cells were seeded at 6×10^4 cells per 24-well in Osteo-Assay Surface plates (Corning, Cat#: 3988XX1) and cultured as above. Cells were further cultured for three days following osteoclasts formation to permit resorption. Osteoclasts numbers and resorptions were detected per manufacturer's instructions thereafter.

MMP-13 immunofluorescence in bone marrow stromal cells and osteoclast cultures was performed. After differentiation, cells were fixed in ice-cold methanol for 7 minutes, washed in 1XPBS prior to blocking for 30 minutes at 25°C using 3% milk in 1XPBS. The cells were then washed with 1XPBS, and incubated with primary antibody (α-mouse MMP-13, 1:250 dilution in blocking solution; Triple Point Biologics, Cat#: RP1-MMP-13) for 1 hour at 25°C. 1XPBS-washed cells were incubated with secondary antibody (Alexa-fluor 488 α-mouse conjugated antibody diluted 1:1000 in blocking solution; Invitrogen, Cat#: A32723; RRID:AB_2633275) for 30 minutes at 25°C. Cells were washed again with 1XPBS and mounted in aqueous mounting media containing phalloidin-488 to visualize actin (1:5000; Invitrogen, Cat#: A12379) and viewed via wide-field fluorescence microscopy.

Real time PCR (RT-PCR), Immunoprecipitation, Western Blot, and Cytokine Array

Total RNA was extracted from cells with TRIzol (Invitrogen) as per manufacturer's instructions. For MMP-13 and Cytokine RNA expression, cDNA was generated by a

standard reverse transcription reaction, and RT-PCR mixtures were generated using SYBR Green reagent (Applied Biosystems, Cat#: 4309155) and reactions were performed and quantified using ABI-7900HT instrument and SDS 2.3 software under manufacturer's instructions (Applied Biosystems; RRID:SCR_018060). Refer to Supplementary Table S1 for RT-PCR primer information.

Standard cell lysis protocols were used to isolate total proteins from cell cultures. For immunoprecipitation experiments, wild-type and MMP-13-null MSCs were washed with 1XPBS and serum-starved in α-MEM for 1 hour at 37°C prior to incubation with fresh α-MEM for 24 hours to generate conditioned media. Conditioned media were pre-cleared with rProtein G with hour-long rocking at 4°C and subject to washes and immunoprecipitation using additional rProtein G (15μL/sample; Invitrogen) and α-mouse CXCL7 antibody at 1μg/0.5mg total protein constituted in 1XPBS to 1mL final volumes (abcam, Cat#: 231102; RRID:AB_949345). Immunoprecipitation was performed at 4°C overnight on rocker and the resulting media was sterilized using sterile filter and centrifugation for use either in *in vitro* cultures or protein blotting. Refer to Supplementary Materials and Methods for isolation of bone marrow supernatant.

For immunoblotting, 25 μg of total protein was electrophoresed and transferred to nitrocellulose. Of note, to blot for less abundant proteins, conditioned media samples were concentrated using Vivaspin-6 3000 MWCO spin filters per manufacturer recommendations (Sartorius, Cat#: VS0691). Transferred blots were blocked for 1 hour at 25°C (1XTBST containing 5% non-fat dairy milk) prior to overnight incubation in primary antibodies: α-mouse MMP-13 at 1:1000 (Triple Point Biologics, Cat#: RP1-MMP-13), and α-mouse CCL-2 (Thermofisher Scientific; Cat#: MA5–17040; RRID:AB_2538512), α-mouse CXCL7 (R&D Systems, Cat#: AF793; RRID:AB_355606), and α-mouse β-Actin at (Cell Signaling, Cat#: 3400S) all at 1:1000. Of note, α-mouse CXCL7 antibody binds to Lys40-Tyr113 and detects active protein. The next day, blots were washed extensively prior to detection with HRP-labeled secondary antibody and ECL using Odyssey Fc Imaging System (LI-COR; RRID:SCR_013430 and RRID:SCR_013715). ELISA was used for the quantification of ICTP (AVIVA Systems Biology, Cat#: OKEH00680) and CXCL7 (RayBiotech, Cat#: ELM-TCK1–5) in *ex vivo* isolated specimens and culture media per manufacturer instructions.

For cytokine array analysis, 18-hour conditioned media from wild-type or MMP-13-null MSCs treated with vehicle or MMP-13i were collected in phenol-free α-MEM after hour-long serum starvation. Cytokine blotting using C2000 Cytokine Array Kit was performed with conditioned media per kit instructions (RayBiotech, Cat#: AAM-CYT-2000–4; RRID:AB_1547202) and detected using Odyssey Fc Imaging System (LI-COR; RRID:SCR_013430 and RRID:SCR_013715).

For proteomic analysis of MMP-13-processed CXCL7, refer to Supplementary Materials and Methods.

In vivo 5TGM1 myeloma studies

For genetic ablation studies, 5TGM1-Luc cells (1×10^6 in 100uL 1XPBS) were tail vein injected into age-matched 6-week old mice that were RAG-2-null or RAG-2-MMP-13 double null (n=20). Multiple myeloma affects men and women equally; therefore, all *in vivo* studies included male and female mice to remove potential sex disparity as a confounding factor in our observations and analyses. Tumor burden was monitored using bioluminescence imaging with IVIS system. Quantitation was performed by secondary research personnel on de-identified and randomized data in a blinded fashion using the Living Image software (Perkin Elmer; RRID:SCR_018621). Murine whole blood was collected weekly by submandibular phlebotomy and serum levels of IgG2b determined by ELISA analysis according to manufacturer's instructions, also in randomized and blinded methods (Bethyl Laboratories, Cat#: A90–109P; RRID:AB_67160 and starter kit Cat#: E101). Mice were euthanized upon reaching the clinical endpoint (hind limb paralysis and/or >10% reduction in body weight). Tumor-bearing tibias were excised and fixed in 10% buffered formalin overnight for further histological analyses.

For pharmacological ablation studies with MMP-13i (Compound 1), age-matched 6-week old immunocompetent KaLwRiJ mice (n=30) were inoculated with 5TGM1-Luc by tail vein route (1×10^6 in 100uL 1XPBS). Both male and female mice were included to account for potential sex disparity as confounding factor. Tumors were allowed 7 days to seed prior to randomization into treatment groups and initiation of daily intraperitoneal injections using vehicle (1XPBS containing 10% DMSO and 10% Tween-80) or MMP-13i at 20mg/Kg body weight (diluted at 5mg/mL in vehicle). Tumor burden was monitored using bioluminescence imaging and quantitated with IVIS Living Image software in blinded methods as described (Perkin Elmer; RRID:SCR_018621). Mice were weighed and monitored for toxicity and well-being daily and euthanized upon reaching the clinical endpoint of hindlimb paralysis. Tumor-bearing tibias were excised and fixed for further histological analyses. All *in vivo* studies were independently repeated.

High-resolution μCT, histology and histomorphometry.

Long-bones were scanned at 6μm increments across 1000μm thickness in the metaphysis 500μm from the growth plate using μ35 instrument for high-resolution μCT analysis (Scanco; RRID:SCR_017119). Tabecular bone volume to total volume ratio (BV:TV) was determined from reconstructed images using manufacturer's software (Scanco; RRID:SCR_017119). Following reconstruction, 3D models of woven bone was built and analyzed by blinded researcher using consistent thresholding on de-identified bone scans data to assess bone quality. For histomorphometry, bones were subsequently decalcified (changes of 14% EDTA pH 7.4 every two days for 3 weeks) and non-sequential FFPE tissue sections were stained with H&E. ImageJ (RRID:SCR_003070) was used for trabecular bone measurements, with the area of analysis beginning 500μm from the growth plate, and extending for 1000μm towards the diaphysis. Osteoclast TRAcP staining was performed to as described previously (Invitrogen, Cat#: 85–0199) on FFPE sections, and the osteoclasts data was manually calculated from multiple 20X fields of view using brightfield microscopy.

Statistical Analysis

Quantified data are represented as mean with SEM when applicable. Statistical analyses were performed by the Moffitt Biostatistics Core when scaling *in vivo* studies to ensure robustness, power and detectable hazard ratios given 5% type I error by a two-sided log-rank test. For statistical analyses of any two treatment groups, Student t test was applied. For statistical analyses of three groups or more, One-way analysis of variance (ANOVA) was performed. Differences were considered significant if $p<0.05$ and noted with asterisks (n.s. represents insignificance).

Results

MMP-13 expression in human multiple myeloma

MMP-13 is highly expressed in the cancer-bone microenvironment[29–31]. Using publicly-available datasets, we initially examined MMP-13 expression levels in isolated CD138+ bone marrow plasma cells derived from healthy control individuals and patients with varying stages of multiple myeloma (n=99; GSE:47552). Analyses suggest that, although MMP-13 was detected, there does not appear to be a difference at the mRNA level between control and patients diagnosed with monoclonal gammopathy of undetermined significance (MGUS), smoldering multiple myeloma (SMM), or symptomatic multiple myeloma (MM) (Fig. 1A). Interestingly, analysis of the Multiple Myeloma Research Foundation (MMRF) CoMMpass cohort dataset (IA14) showed no MMP-13 expression in CD138+ myeloma cells in 56% of patients (433 of 770). Of the patients that did express MMP-13, albeit at very low levels, myeloma-derived MMP-13 did not correlate with progression free survival but did correlate with overall survival (Supplementary Fig. S1A and B).

We performed similar analyses on additional collagenases (MMP-1, -8) expressed by CD138+ cells and found MMP-1 is expressed at significantly higher levels in active multiple myeloma but observed no differences in MMP-8 expression (Supplementary Fig. S2A and B). We and others have shown that MMP expression is often induced in the surrounding stroma[32]. Cancer-derived stimuli including interleukins and PTHrP induce MMP-13 expression in bone stroma[20, 30, 33]. In keeping with this observation, we identified that MMP-1, -8 and -13 expression was significantly enhanced in primary bone marrow-derived incubated with human multiple myeloma cells (MM.1S) (Fig. 1B and Supplementary Fig. S2C and D; GSE:46053, n=37)[18], [34]. Of these MMPs, MMP-13 expression is largely confined to the skeletal tissues making it an attractive therapeutic target as opposed to systemically-expressed MMPs. We therefore focused on identifying the cellular sources of MMP-13 in human myeloma biopsies (Fig. 1C) and consistently observed positivity in the stromal compartment, specifically in cuboidal bone-lining cells compared to CD138-stained myeloma cells (Fig. 1D). Interestingly, and in keeping with previous reports[19, 35], we detected MMP-13 positivity in the bone matrix itself within bone cement lines (Fig. 1C and D).

Murine MMP-13 expression in the multiple myeloma-bone microenvironment.

Given the high level of expression of MMP-13 by bone-lining cells in human myeloma specimens and its potential role in processing type I collagen, we hypothesized that

stromal MMP-13 contributes to myeloma disease progression. Addressing the contribution of stromal genes to multiple myeloma progression *in vivo* has been challenging but we addressed this issue by generating RAG-2/MMP-13 double null animals that are receptive to engraftment with the murine multiple myeloma cell line 5TGM1[23]. In keeping with our findings in human tissues, immunohistochemical analysis of wild-type (WT) and MMP-13-null (MMP-13$^{-/-}$) tissues demonstrated that MMP-13 expression was largely confined to bone-lining cells and the cement lines of the bone matrix, while, as expected, MMP-13 expression was not detected in MMP-13-null animals (Supplementary Fig. S3A) [6]. RT-PCR and immunofluorescence consistently demonstrated the presence of MMP-13 in wild-type MSCs but not osteoclasts (Supplementary Fig. S3B and C). We also observed that 5TGM1 conditioned media (RPMI) significantly increased MMP-13 mRNA expression in wild-type MSCs compared to controls (RPMI media alone) (Supplementary Fig. S3D) that was in keeping with human analyses (Fig. 1B). In contrast, RT-PCR revealed variable MMP-13 expression across mouse and human myeloma cell lines (Supplementary Figure. S4).

Host-derived MMP-13 impacts multiple myeloma overall survival

Since we observed robust expression of MMP-13 in the bone stroma, we next determined whether host-derived MMP-13 contributes to myeloma progression *in vivo*. In three independent studies, wild-type or MMP-13-null animals (n=10/group) were inoculated with luciferase-expressing 5TGM1 cells. Tumor burden was monitored weekly by bioluminescence imaging. Log-scale analysis showed no difference between the groups in regards to tumor growth rate (Fig. 2A and B). Measurement of weekly serum IgG2b concentrations confirmed bioluminescence data (Fig. 2C). Surprisingly, despite no apparent difference in tumor growth rates, overall survival in the MMP-13-null multiple myeloma-bearing mice was significantly higher than that of the wild-type group with median survival times of 43 and 39 days, respectively (p=0.0011; Fig. 2D). Of note, for the 5TGM1 model, this increase in overall survival is in keeping with reports for approved myeloma therapies such as melphalan, bortezomib and bisphosphonates[36, 37]. Immunohistochemical analysis for IgG2b in *ex vivo* myeloma-bearing bone tissue confirmed that the multiple myeloma burden in the wild-type and MMP-13-null groups was similar (Fig. 2E).

MMP-13 contributes to multiple myeloma induced bone loss

MMP-13-null mice have hypertrophic growth plates and delays in endochondral ossification during skeletal development[6, 38], while adult mice have increased trabecular bone volume [6, 39]. Using high-resolution μCT, we confirmed increased trabecular bone: total volume (BV:TV) in age-matched (12-week-old) tumor-naïve MMP-13-null mice compared to tumor-naïve wild-type controls (Fig. 2F). The age of these control mice was chosen to correspond with the approximate age at which the myeloma-bearing mice reached their clinical endpoint. To determine multiple myeloma BV:TV differences between the groups, we used the ratios obtained from tumor-naïve mice as a means of normalization (Tumor BV:TV). Using this approach, we observed that bone loss was significantly reduced in the MMP-13-null mice compared to their wild-type counterparts (Fig. 2G). We also noted significant differences in trabecular bone (Tr.) parameters such as spacing, patterning factor, thickness and number in MMP-13-null myeloma-bearing animals compared to wild type,

results that are consistent with reduced bone loss in the MMP-13-null myeloma-bearing animals (Fig. 2H–K). Analysis of BV:TV in non-sequential sections from tumor-bearing tibia confirmed μCT results (Fig. 3A and B). To identify the potential causes for reduced bone volume in the MMP-13-null mice, we examined MMP-13's ability to process type I collagen. MMP processing of type I collagen into cross-linked carboxyterminal telopeptide of type I collagen (ICTP) is distinguishable from cathepsin K activity which generates N- and C-terminal peptides (NTX, CTX)[12, 40, 41]. Using an ICTP-specific ELISA, we observed no differences between wild-type versus MMP-13-null bone marrow supernatants derived from multiple myeloma-bearing animals (Supplementary Fig. S5). We also examined and found no differences in numbers of osteoclasts/mm of tumor-bone interface or size between the wild-type and MMP-13-null groups despite osteoclasts' key role in bone resorption (Fig. 3C–E). Since these analyses were done at study endpoint, temporal differences between the groups may not have been observable. We therefore repeated the study and harvested tumor-bearing tibias at day 21 post inoculation (Supplementary Fig. S6A and B). Again, we observed no differences in osteoclast number between the groups (Supplementary Fig. S6C).

MMP-13 regulates osteoclastogenesis and function

Given there was no difference in osteoclast size *in vivo* at either study mid- or end-point, we hypothesized that temporal differences in osteoclast formation and/or activity may be responsible for the slower resorption in the MMP-13-null myeloma-bearing animals. We therefore conducted *in vitro* studies to test this hypothesis. Since osteoclasts do not express MMP-13 (Supplementary Fig. S3C), we performed osteoclastogenic assays over 7 days using whole bone marrow-derived co-cultures from wild-type and MMP-13-null mice. Our *in vitro* data demonstrate significantly more but smaller multinucleated osteoclasts in the MMP-13-null cultures (Fig. 4A–C). Further, when normalizing to osteoclast numbers, we also observed MMP-13-null osteoclasts were less resorptive than wild-type controls (Fig. 4D and E). Our *in vitro* data on osteoclast numbers at day 7 contrasted previous reports showing fewer numbers of osteoclasts at day 5[19, 29]. We therefore more closely examined temporal osteoclast formation rates and found that wild-type osteoclast formation peaks one day earlier than MMP-13-null osteoclasts, and that relative osteoclast numbers between groups vary significantly depending on assay duration (Fig. 4F and G). Taken together, these results demonstrate that stromal MMP-13 is critical for efficient formation of osteoclasts and their activity.

MSC-derived MMP-13 mediates secretion of key factors driving osteoclastogenesis

Since we observed no differences in type I collagen turnover between myeloma-bearing wild-type and MMP-13-null mice but did note defects in osteoclast formation rates and function, we next examined whether MMP-13 ablation altered production/bioavailability of factors that could influence osteoclast behavior. To this end, we focused on MSCs since we found this population to be a major source of MMP-13. We generated conditioned media from wild-type and MMP-13-null MSCs and performed cytokine array analysis that identified differences in factors potentially responsible for regulating osteoclast behavior (Fig. 5A). As a control, we included a novel selective inhibitor of MMP-13 catalytic activity (MMP-13i)[26]. Incubation of wild-type MSCs with MMP-13i mirrored decreases noted

with MMP-13-null MSCs. Importantly, these results indicated MMP-13 catalytic, rather than non-catalytic activity regulated MSC cytokine/growth factor bioavailability (Supplementary Fig. S7A and B). RT-PCR analysis was used to validate cytokine array data at the transcript level (Fig. 5B). Using a candidate approach, we focused on CXCL7 since, in MMP-13-null MSCs, it had elevated mRNA levels but reduced active protein levels in the conditioned media (Fig. 5A and B). CXCL7 is proteolytically activated from the latent pro-platelet basic protein (PPBP) by MMP-3, and cathepsin G[42–44]. Interestingly, we also observed that MMP-3 expression was increased at the transcriptional and protein level in MMP-13-null MSCs, but this increase was not sufficient to compensate for MMP-13 loss and rescue bioavailability of active CXCL7 (Fig. 5A and B). Western blot analysis corroborates CXCL7 cytokine array results in both MSC lysate and conditioned media (Fig. 5C). Notably, treatment of wild-type MSCs with MMP-13i reduced the amount of secreted CXCL7 to that noted with the MMP-13-null MSCs, further supporting MMP-13 control of CXCL7 levels (Fig. 5D). Proteolytically-activated CXCL7 promotes osteoclastogenesis but has not been described as an MMP-13 substrate[45, 46]. Immunoblotting demonstrated processing of recombinant human CXCL7 full-length peptide upon incubation with recombinant human active MMP-13 (Fig. 5E and Supplementary Fig. S8A). Human and mouse CXCL7 share 79.3% homology and therefore, this was verified with murine MMP-13 and CXCL7 (Supplementary Fig. S8B). Mass-spectrometry identified novel MMP-13 direct cleavage sites in both human and murine full-length CXCL7 pro-peptides (Supplementary Fig. 8A and B). Specifically, human CXCL7 was predominantly processed at Glu^{27}, which is one amino acid away from the canonical activating cleavage site observed with Cathepsin G[45, 46]. Importantly, MMP-13-processed CXCL7 significantly increased osteoclast formation in MMP-13-null cultures (Supplementary Fig. 8C). We also noted that the addition of exogenous recombinant MMP-13 alone partially rescued CXCL7 levels in MMP-13-null whole bone marrow co-cultures (Supplementary Fig. 9A and B). To further test the importance of MSC-derived CXCL7 in osteoclast formation, we immunodepleted CXCL7 from wild-type MSC conditioned media and observed significantly-reduced wild-type osteoclast numbers that were similar to those induced by MMP-13-null MSC conditioned media (Fig. 5F and G). These results indicate that MMP-13 regulation of CXCL7 bioavailability from MSC is important for enhancing osteoclast formation.

Pharmacological MMP-13 ablation with novel inhibitor improves overall survival

Recent reports demonstrated that myeloma-derived MMP-13 can contribute to osteoclast fusogenesis in a non-catalytic manner. Our data thus far indicates that bone stroma-derived MMP-13 catalytic activity is important for regulating the bioavailability of important osteoclastogenic factors such as CXCL7. To further explore whether MMP-13 activity was necessary for osteoclast formation, we tested a series of MMP-13-selective inhibitors with nM-range IC_{50}'s (Compound 1, 2 and 4). In previous studies, these compounds were shown to selectively target the catalytic domain of MMP-13 (Supplementary Fig. S10A and B)[25, 26, 47]. Of these reagents, we observed that Compound 1 potently suppressed wild-type osteoclast formation *in vitro* at concentrations <100 nM compared to the other inhibitors (Fig. 6A). The remainder studies were therefore conducted with Compound 1, designated as MMP-13i. MMP-13 inhibition by MMP-13i compromised the viability of myeloma cell lines (MM1.S, 5TGM1, OPM2, U266) albeit at concentrations >1 μM (Fig. 6B).

Interestingly, MMP-13i did not affect the viability of MSCs or CD11b-isolated monocytes at concentrations <5 μM (Supplementary Fig. S10C).

To determine the *in vivo* efficacy of the MMP-13i, 6-week-old immunocompetent syngeneic KaLwRiJ mice (n=30) were inoculated with 5TGM1-Luc cells to establish skeletal lesions. After 7 days, mice were randomized into vehicle control and MMP-13i groups. Bioluminescence imaging results demonstrated a delay in myeloma growth over time (Fig. 6C). Similar to our genetic studies, we also observed a significant increase in overall survival in the MMP-13i treated group compared to vehicle control (median survival times 35 versus 42 days, respectively, Fig. 6D). We noted that MMP-13i treatment resulted in a trend of decreased osteoclast numbers (Supplementary Fig. S11A and B) with no difference in BV:TV ratios between the vehicle control and MMP-13i treatment group in tumor-bearing mice. MMP-13i treatment of tumor-naïve mice did however demonstrate an increase in BV:TV compared to controls (Fig. 6E). Collectively, based on these data, our working model is that that multiple myeloma induces MMP-13 in the surrounding bone stroma and that MMP-13 processing of factors such as CXCL7 enhance osteoclast formation rates leading to increased myeloma-induced bone disease. We propose that inhibition of MMP-13 activity can block this mechanism and thereby significantly enhance overall survival (Fig. 6F).

Discussion

Multiple myeloma induces systemic skeletal lesions that greatly impact patient quality of life. The vicious cycle of myeloma-bone interaction increases bioavailability of cytokines and growth factors that enhance tumor growth and contribute to therapy resistance[1, 48]. Mechanisms governing reciprocal interactions between the myeloma and surrounding bone microenvironment are therefore of potential therapeutic importance. Here, we have shown that MMP-13 ablation from the host stroma significantly extended overall survival of myeloma-bearing mice. Interestingly, this effect appears to be due to MSC-derived MMP-13 regulating the availability of multiple cytokines including CXCL7 that control osteoclast formation and activity rather than collagen turnover. Importantly, our studies show that this effect depends on MMP-13 catalytic activity since an MMP-13-selective inhibitor could significantly extend overall survival in multiple myeloma-bearing mice.

Although our mice are systemically null for MMP-13, the studies herein have focused primarily on MSC- and osteoblast-derived MMP-13 given our immunolocalization data in human and mouse multiple myeloma samples. Consistent with previous reports, this lineage is a major source of MMP-13 with noted expression in chondrocytes and osteocytes[39]. Underscoring the importance of MMP-13 in osteoblast biology, tissue-specific knockout of MMP-13 using type Iα collagen promoter-driven CRE recombinase recapitulates the developmental bone phenotypes noted in systemic MMP-13-null mice[39]. Importantly, MMP-2- and -14-null mice also exhibit bone phenotypes, but they fail to compensate for the loss of MMP-13 indicating a distinct role for this protease in bone remodeling. Cancer cells also induce MMP-13 in MSCs and osteoblasts (Fig. 1B and Supplementary Fig. S3D) [18, 29]. To date, however, few studies have been able to examine whether stromal genes of interest such as MMP-13 impact myeloma progression, particularly *in vivo*. This is largely due to the limited availability of genetically-engineered models that are receptive to

myeloma engraftment[49]. Here, using RAG-2/MMP-13 double null mice, our data show that stromal MMP-13 contributes to myeloma-induced bone destruction by regulating the bioavailability of non-matrix molecules such as CXCL7 that impact osteoclast recruitment, formation and function as opposed to processing type I collagen. It is also important to note that several MMP-deficient mice carry a caspase-11 passenger mutation, including the MMP-13-null mice used in this study[50]. However, the *in vitro* and *in vivo* data obtained with our MMP-13-selective inhibitor support, in large part, those obtained with the RAG-2/MMP-13-null mice indicating negligible if any caspase-11 contribution. The similarities between the MMP-13-null studies in immunocompromised mice and MMP-13 inhibitor studies in immunocompetent KaLwRiJ mice also suggests immune cells such as T-cells may not be involved in the effects mediated by host MMP-13[51, 52].

Ex vivo, our analysis of MSC conditioned media revealed the regulation of several non-matrix molecules that have reported roles in controlling osteoclast biology including CXCL7[45, 46]. Expressed as an inactive pro-peptide (PPBP), CXCL7 undergoes successive rounds of proteolytic cleavage to eventually yield the active 7.6 kDa peptide[53]. Here, we report for the first time that MMP-13 regulates CXCL7 bio-activation and availability and is critical for MSC-induced osteoclast formation. Our mass spectrometry data demonstrated MMP-13-directed CXCL7 cleavage sites resembling that of canonical activation sites by Cathepsin G processing (Supplementary Fig. 7A and B). We also noted that MMP-13 could process CXCL7, at other distinct sites, albeit that these cleavage events were noted less frequently than the processing at Glu^{27}. These findings warrant further investigation into smaller CXCL7 fragments and how post-translational modification by MMP-13 potentially regulates cellular behavior in the tumor-bone microenvironment. Previously, we have shown this to be the case of parathyroid hormone related protein (PTHrP), a potent hormone involved in controlling cancer-induced osteolysis[33]. While we acknowledge the currently-unknown functional nature of the shorter fragments, our osteoclastogenesis treatment assays nonetheless support MMP-13-processed CXCL7 retains osteoclastogenic activity (Supplementary Fig. S8).

While not examined here, it is also possible that the MMP-13-CXCL7 interaction could influence the behavior of other cell types in the myeloma-bone microenvironment. For example, CXCL7 has been identified as a potent mediator of neutrophil chemoattraction and activation in various pathologies in addition to noted roles in osteoclastogenesis[42, 45]. Further, we do not discount that myeloma- or MSC-derived MMP-13 can regulate the bioavailability of CXCL7 expressed by other cell types/platelets in the bone marrow microenvironment. While MMP-3 and cathepsin G have been shown to participate in proteolytic activation of PPBP, we posit MMP-13 is a key regulator of CXCL7 expression and activity given the low levels of CXCL7 detected in the conditioned media derived from MMP-13-null MSCs and wild type MSCs treated with MMP-13i[53] and our data showing MMP-13 can directly process CXCL-7 to enhance its osteoclastogenic activity. Of note, MMP-3 expression is increased in MMP-13-null MSCs (Fig. 5A) and MMP-3 has been reported to activate latent MMP-13[12]. However, the increased levels of MMP-3 expression are insufficient to rescue protein levels of active CXCL7 supporting a role for MMP-13 in the process. While we noted the dysregulation of other factors in the MMP-13-null MSC

conditioned media that can impact osteoclast biology, immune depletion of CXCL7 from conditioned media significantly inhibited the process.

Collectively, our study demonstrates a role for the catalytic activity of stromal MMP-13 in multiple myeloma progression and overall survival. This is evidenced by our data examining CXCL7 processing and our *in vitro* and *in vivo* MMP-13i data. Additionally, the detected differences in non-matrix factors in MMP-13-null MSC conditioned media reinforce a role for MMP-13 catalytic activity. This position is further supported by data showing that when wild-type MSCs are treated with a MMP-13-selective inhibitor, the profile and levels of down-regulated growth factors mirror those observed with the MMP-13-null MSCs (Supplementary Fig. S7A). In agreement, published studies have also demonstrated MMP-13 catalytic regulation of the MC3T3 osteoblast degradome[18, 54].

As stated, in the context of skeletal malignancies, MMP-13 can also be derived from cancer cells[15, 55, 56]. Indeed, our own studies show expression of MMP-13 in CD138+ cells, and our analysis of the MMRF dataset also correlated MMP-13 status with overall survival (Fig. 1D, 5B–C and Supplementary Fig. S1B). Interestingly, we noted that CD138+ myeloma cell MMP-13 expression did not correlate with disease staging in publicly-available datasets. Previous reports have shown that MMP-13 derived from multiple myeloma cells (5TGM1) can contribute to osteoclast fusogenesis and that this effect is independent of the catalytic activity of MMP-13[15]. This non-catalytic role for MMPs in osteoclast fusion has also been reported for MMP-14[57]. In our experiments, 5TGM1-derived MMP-13 did not compensate for the loss of MMP-13 in the bone stroma compartment suggesting spatial localization may be important. Our results with MMP-13-selective inhibitors further support a catalytic role for host-derived MMP-13 in contributing to disease progression. The selectivity of the inhibitor was supported in experiments showing that the addition of the MMP-13i to MMP-13-null MSCs had no further effect on either downregulated or upregulated cytokines or growth factors (Supplementary Fig. S7B). MMP inhibitors as a modality to treat cancer were not successful in the clinical setting because of their largely broad-spectrum nature and dose-limiting side effects[58]. However, the relatively-deep catalytic pocket of MMP-13 and restricted tissue expression of the protease to the tumor-bone microenvironment make it an ideal candidate for selective inhibition[59–62]. Here, using a MMP-13-selective inhibitor (IC_{50} of 2.7nM), we demonstrate inhibition of MMP-13 activity *in vivo* recapitulated the effects observed in our MMP-13-null studies in regard to significantly improving overall survival in myeloma-bearing mice. Importantly, both genetic and pharmacologic ablation of MMP-13 yielded comparable improved overall survival in mice as does standard of care treatments.

However, it is important to note differences between the genetic and pharmacological approaches taken in this study. For example, we did not observe a protective effect on myeloma-induced bone destruction with the MMP-13i. We suspect that this is due to the short duration (between 31–54 days) of treatment compared to genetically null mice where MMP-13 is absent from birth. Therefore, over a longer period, this protective effect of inhibiting MMP-13 on cancer-induced bone disease would be more manifest. Supporting this position is the fact that treatment of wild-type tumor-naïve mice for the same period of time significantly increases bone volume (Fig. 6E). While we observed

a decrease in osteoclast numbers in MMP-13 inhibitor-treated animals, this reduction did not reach statistical significance. Pharmacokinetic/pharmacodynamics studies have not been performed with the MMP-13i and so it is possible that higher doses or improving inhibitor half-life *in vivo* could more potently protect against osteoclastogenesis and myeloma-associated bone disease. Importantly, we do not rule out that the non-catalytic function of MMP-13 in osteoclast fusion may also explain why a more dramatic effect on osteoclast numbers between the MMP-13 inhibitor and vehicle control groups was not noted. Nevertheless, given the increase in overall survival noted in the MMP-13i cohort, we posit that MMP-13 catalytic activity plays an important role in the progression of the disease. In support of targeting MMP-13 activity therapeutically for skeletal malignancies, previous studies with MMP-13 inhibitors such as 5-(4-phenoxy)-5-(2-methoxyethyl)-pyrimidine-2,4,6 (1H,3H,5H)-trione (IC_{50} = 0.57nM) demonstrated efficacy in a bone-metastatic breast cancer model by mitigating metastatic tumor burden and tumor-induced bone disease[63, 64]. Ongoing studies by our group will leverage MMP-13 specific fluorescent triple-helical peptides (fTHP) for analysis of MMP-13 catalytic activity *in vivo* or *ex vivo* and should help delineate between the potentially catalytic and non-catalytic functions of this enzyme[63, 65].

In conclusion, we have shown that MMP-13 contributes to the overall survival of multiple myeloma-bearing animals. Our data demonstrate that this is due to slower rates of bone turnover that is not related to the ability of MMP-13 to process type I collagen, but rather the regulation of bioavailable CXCL7 that in turn is critical for osteoclast formation and function. We further demonstrate the efficacy of a novel highly-selective MMP-13 inhibitor for the treatment of the disease using an immunocompetent preclinical animal model. In conclusion, we have shown that stromal MMP-13 activity contributes to multiple myeloma reduced overall survival and that MMP-13 inhibition is a tractable and valid target for the treatment of this currently incurable disease.

Supplementary Material

Refer to Web version on PubMed Central for supplementary material.

Acknowledgments

MMP-13-null mice on a C57BL/6 background were kindly provided by Dr. Stephen M. Krane, MGH. Luciferase-labeled myeloma cells (5TGM1-Luc) were obtained from Dr. Toshiyuki Yoneda via University of Texas, Health Science Center at San Antonio, TX. Luciferase-labeled U266 cells (U266-Luc) were obtained from Dr. Steven Grant at the University of Virginia, VA. MMP-13 inhibitor (MMP-13i) is an invention of Dr. Gregg B. Fields, William R. Roush, Jun Yong Choi and Rita Fuerst (US Patent Appl. US20200181095A1, June 11, 2020).

Grant Support: These studies were supported in part by R01-CA239214-01 (CCL) and R21-CA191981-01A1 (CCL).

References

1. Shay G, Hazlehurst L, and Lynch CC, Dissecting the multiple myeloma-bone microenvironment reveals new therapeutic opportunities. J Mol Med (Berl), 2016. 94(1): p. 21–35. [PubMed: 26423531]
2. Brown JE and Coleman RE, Denosumab in patients with cancer-a surgical strike against the osteoclast. Nat Rev Clin Oncol, 2012. 9(2): p. 110–8. [PubMed: 22231759]

3. Lu J, et al. , Advances in the discovery of cathepsin K inhibitors on bone resorption. J Enzyme Inhib Med Chem, 2018. 33(1): p. 890–904. [PubMed: 29723068]
4. Bossard MJ, et al. , Proteolytic activity of human osteoclast cathepsin K. Expression, purification, activation, and substrate identification. J Biol Chem, 1996. 271(21): p. 12517–24. [PubMed: 8647860]
5. Bromme D, et al. , Human cathepsin O2, a matrix protein-degrading cysteine protease expressed in osteoclasts. Functional expression of human cathepsin O2 in Spodoptera frugiperda and characterization of the enzyme. J Biol Chem, 1996. 271(4): p. 2126–32. [PubMed: 8567669]
6. Inada M, et al. , Critical roles for collagenase-3 (Mmp13) in development of growth plate cartilage and in endochondral ossification. Proc Natl Acad Sci U S A, 2004. 101(49): p. 17192–7. [PubMed: 15563592]
7. Mosig RA, et al. , Loss of MMP-2 disrupts skeletal and craniofacial development and results in decreased bone mineralization, joint erosion and defects in osteoblast and osteoclast growth. Hum Mol Genet, 2007. 16(9): p. 1113–23. [PubMed: 17400654]
8. Inoue K, et al. , A crucial role for matrix metalloproteinase 2 in osteocytic canalicular formation and bone metabolism. J Biol Chem, 2006. 281(44): p. 33814–24. [PubMed: 16959767]
9. Mosig RA and Martignetti JA, Loss of MMP-2 in murine osteoblasts upregulates osteopontin and bone sialoprotein expression in a circuit regulating bone homeostasis. Dis Model Mech, 2013. 6(2): p. 397–403. [PubMed: 22917927]
10. Holmbeck K, et al. , MT1-MMP: a tethered collagenase. J Cell Physiol, 2004. 200(1): p. 11–9. [PubMed: 15137053]
11. Taylor SH, et al. , Matrix metalloproteinase 14 is required for fibrous tissue expansion. Elife, 2015. 4: p. e09345. [PubMed: 26390284]
12. Knauper V, et al. , Biochemical characterization of human collagenase-3. J Biol Chem, 1996. 271(3): p. 1544–50. [PubMed: 8576151]
13. Hattori N, et al. , MMP-13 plays a role in keratinocyte migration, angiogenesis, and contraction in mouse skin wound healing. Am J Pathol, 2009. 175(2): p. 533–46. [PubMed: 19590036]
14. Botos I, et al. , Structure of recombinant mouse collagenase-3 (MMP-13). J Mol Biol, 1999. 292(4): p. 837–44. [PubMed: 10525409]
15. Fu J, et al. , Multiple myeloma-derived MMP-13 mediates osteoclast fusogenesis and osteolytic disease. J Clin Invest, 2016. 126(5): p. 1759–72. [PubMed: 27043283]
16. Wahlgren J, et al. , Expression and induction of collagenases (MMP-8 and -13) in plasma cells associated with bone-destructive lesions. J Pathol, 2001. 194(2): p. 217–24. [PubMed: 11400151]
17. Fu J, et al. , Multiple myeloma-derived MMP-13 mediates osteoclast fusogenesis and osteolytic disease. The Journal of clinical investigation, 2016. 126(5): p. 1759–1772. [PubMed: 27043283]
18. Morrison C, et al. , Microarray and proteomic analysis of breast cancer cell and osteoblast co-cultures: role of osteoblast matrix metalloproteinase (MMP)-13 in bone metastasis. J Biol Chem, 2011. 286(39): p. 34271–85. [PubMed: 21784845]
19. Nakamura H, et al. , Immunolocalization of matrix metalloproteinase-13 on bone surface under osteoclasts in rat tibia. Bone, 2004. 34(1): p. 48–56. [PubMed: 14751562]
20. Weisser J, et al. , Four distinct chondrocyte populations in the fetal bovine growth plate: highest expression levels of PTH/PTHrP receptor, Indian hedgehog, and MMP-13 in hypertrophic chondrocytes and their suppression by PTH (1–34) and PTHrP (1–40). Exp Cell Res, 2002. 279(1): p. 1–13. [PubMed: 12213208]
21. Tang SY, et al. , Matrix metalloproteinase-13 is required for osteocytic perilacunar remodeling and maintains bone fracture resistance. J Bone Miner Res, 2012. 27(9): p. 1936–50. [PubMed: 22549931]
22. Lwin ST, et al. , A loss of host-derived MMP-7 promotes myeloma growth and osteolytic bone disease in vivo. Mol Cancer, 2017. 16(1): p. 49. [PubMed: 28241871]
23. Fowler JA, et al. , A murine model of myeloma that allows genetic manipulation of the host microenvironment. Dis Model Mech, 2009. 2(11–12): p. 604–11. [PubMed: 19779066]
24. Mori Y, et al. , Anti-alpha4 integrin antibody suppresses the development of multiple myeloma and associated osteoclastic osteolysis. Blood, 2004. 104(7): p. 2149–54. [PubMed: 15138161]

25. Fuerst R, et al. , Development of matrix metalloproteinase-13 inhibitors - A structure-activity/structure-property relationship study. Bioorg Med Chem, 2018. 26(18): p. 4984–4995. [PubMed: 30249495]
26. Choi JY, et al. , Structure-Based Design and Synthesis of Potent and Selective Matrix Metalloproteinase 13 Inhibitors. J Med Chem, 2017. 60(13): p. 5816–5825. [PubMed: 28653849]
27. Zhu H, et al. , A protocol for isolation and culture of mesenchymal stem cells from mouse compact bone. Nat Protoc, 2010. 5(3): p. 550–60. [PubMed: 20203670]
28. Yusop N, et al. , Isolation and Characterisation of Mesenchymal Stem Cells from Rat Bone Marrow and the Endosteal Niche: A Comparative Study. Stem Cells Int, 2018. 2018: p. 6869128. [PubMed: 29765418]
29. Pivetta E, et al. , MMP-13 stimulates osteoclast differentiation and activation in tumour breast bone metastases. Breast Cancer Res, 2011. 13(5): p. R105. [PubMed: 22032644]
30. Ibaragi S, et al. , Parathyroid hormone-related peptide regulates matrix metalloproteinase-13 gene expression in bone metastatic breast cancer cells. Anticancer Res, 2010. 30(12): p. 5029–36. [PubMed: 21187486]
31. Lynch CC, et al. , MMP-7 promotes prostate cancer-induced osteolysis via the solubilization of RANKL. Cancer Cell, 2005. 7(5): p. 485–96. [PubMed: 15894268]
32. Lynch CC, Matrix metalloproteinases as master regulators of the vicious cycle of bone metastasis. Bone, 2011. 48(1): p. 44–53. [PubMed: 20601294]
33. Frieling JS, et al. , Matrix metalloproteinase processing of PTHrP yields a selective regulator of osteogenesis, PTHrP1–17. Oncogene, 2017. 36(31): p. 4498–4507. [PubMed: 28368420]
34. Garcia-Gomez A, et al. , Transcriptomic profile induced in bone marrow mesenchymal stromal cells after interaction with multiple myeloma cells: implications in myeloma progression and myeloma bone disease. Oncotarget, 2014. 5(18): p. 8284–305. [PubMed: 25268740]
35. Blavier L and Delaisse JM, Matrix metalloproteinases are obligatory for the migration of preosteoclasts to the developing marrow cavity of primitive long bones. J Cell Sci, 1995. 108 (Pt 12): p. 3649–59. [PubMed: 8719871]
36. Wang Q, et al. , Therapeutic effects of CSF1R-blocking antibodies in multiple myeloma. Leukemia, 2018. 32(1): p. 176–183. [PubMed: 28626216]
37. Croucher PI, et al. , Zoledronic acid treatment of 5T2MM-bearing mice inhibits the development of myeloma bone disease: evidence for decreased osteolysis, tumor burden and angiogenesis, and increased survival. J Bone Miner Res, 2003. 18(3): p. 482–92. [PubMed: 12619933]
38. Leeman MF, Curran S, and Murray GI, The structure, regulation, and function of human matrix metalloproteinase-13. Crit Rev Biochem Mol Biol, 2002. 37(3): p. 149–66. [PubMed: 12139441]
39. Stickens D, et al. , Altered endochondral bone development in matrix metalloproteinase 13-deficient mice. Development, 2004. 131(23): p. 5883–95. [PubMed: 15539485]
40. Fields GB, Van Wart HE, and Birkedal-Hansen H, Sequence specificity of human skin fibroblast collagenase. Evidence for the role of collagen structure in determining the collagenase cleavage site. J Biol Chem, 1987. 262(13): p. 6221–6. [PubMed: 3032960]
41. Garnero P, et al. , The type I collagen fragments ICTP and CTX reveal distinct enzymatic pathways of bone collagen degradation. J Bone Miner Res, 2003. 18(5): p. 859–67. [PubMed: 12733725]
42. Schenk BI, et al. , Platelet-derived chemokines CXC chemokine ligand (CXCL)7, connective tissue-activating peptide III, and CXCL4 differentially affect and cross-regulate neutrophil adhesion and transendothelial migration. J Immunol, 2002. 169(5): p. 2602–10. [PubMed: 12193731]
43. Ju D and Kosir MA, Abstract 5163: MMP3 increases expression of CXCL7. Cancer Research, 2013. 73(8 Supplement): p. 5163–5163. [PubMed: 23946472]
44. Kruidenier L, et al. , Myofibroblast matrix metalloproteinases activate the neutrophil chemoattractant CXCL7 from intestinal epithelial cells. Gastroenterology, 2006. 130(1): p. 127–36. [PubMed: 16401476]
45. Goto Y, et al. , CXCR4(+) CD45(−) Cells are Niche Forming for Osteoclastogenesis via the SDF-1, CXCL7, and CX3CL1 Signaling Pathways in Bone Marrow. Stem Cells, 2016. 34(11): p. 2733–2743. [PubMed: 27339271]

46. Tsuru M, et al. , Ubiquitin-dependent proteolysis of CXCL7 leads to posterior longitudinal ligament ossification. PLoS One, 2018. 13(5): p. e0196204. [PubMed: 29782494]
47. Fields GB, New strategies for targeting matrix metalloproteinases. Matrix Biol, 2015. 44–46: p. 239–46.
48. Dalton WS, et al. , Targeting the bone marrow microenvironment in hematologic malignancies. Seminars in hematology, 2004. 41(2 Suppl 4): p. 1–5.
49. Aiken A and Khokha R, Unraveling metalloproteinase function in skeletal biology and disease using genetically altered mice. Biochim Biophys Acta, 2010. 1803(1): p. 121–32. [PubMed: 19616584]
50. Vanden Berghe T, et al. , Passenger Mutations Confound Interpretation of All Genetically Modified Congenic Mice. Immunity, 2015. 43(1): p. 200–9. [PubMed: 26163370]
51. Rossi M, et al. , Mouse models of multiple myeloma: technologic platforms and perspectives. Oncotarget, 2018. 9(28): p. 20119–20133. [PubMed: 29732008]
52. Alici E, et al. , Visualization of 5T33 myeloma cells in the C57BL/KaLwRij mouse: establishment of a new syngeneic murine model of multiple myeloma. Exp Hematol, 2004. 32(11): p. 1064–72. [PubMed: 15539084]
53. Gleissner CA, von Hundelshausen P, and Ley K, Platelet chemokines in vascular disease. Arterioscler Thromb Vasc Biol, 2008. 28(11): p. 1920–7. [PubMed: 18723831]
54. Eckhard U, et al. , Active site specificity profiling datasets of matrix metalloproteinases (MMPs) 1, 2, 3, 7, 8, 9, 12, 13 and 14. Data Brief, 2016. 7: p. 299–310. [PubMed: 26981551]
55. Kudo Y, et al. , Matrix metalloproteinase-13 (MMP-13) directly and indirectly promotes tumor angiogenesis. J Biol Chem, 2012. 287(46): p. 38716–28. [PubMed: 22992737]
56. Kotepui M, et al. , Differential expression of matrix metalloproteinase-13 in association with invasion of breast cancer. Contemp Oncol (Pozn), 2016. 20(3): p. 225–8. [PubMed: 27647987]
57. Gonzalo P, et al. , MT1-MMP is required for myeloid cell fusion via regulation of Rac1 signaling. Dev Cell, 2010. 18(1): p. 77–89. [PubMed: 20152179]
58. Shay G, Lynch CC, and Fingleton B, Moving targets: Emerging roles for MMPs in cancer progression and metastasis. Matrix Biol, 2015. 44–46: p. 200–6.
59. Zhang B, et al. , Tumor-derived matrix metalloproteinase-13 (MMP-13) correlates with poor prognoses of invasive breast cancer. BMC Cancer, 2008. 8: p. 83. [PubMed: 18373849]
60. Johansson N, et al. , Collagenase-3 (MMP-13) is expressed by tumor cells in invasive vulvar squamous cell carcinomas. Am J Pathol, 1999. 154(2): p. 469–80. [PubMed: 10027405]
61. Balbin M, et al. , Expression and regulation of collagenase-3 (MMP-13) in human malignant tumors. APMIS, 1999. 107(1): p. 45–53. [PubMed: 10190279]
62. Yamamoto K, et al. , MMP-13 is constitutively produced in human chondrocytes and co-endocytosed with ADAMTS-5 and TIMP-3 by the endocytic receptor LRP1. Matrix Biol, 2016. 56: p. 57–73. [PubMed: 27084377]
63. Shah M, et al. , An MMP13-selective inhibitor delays primary tumor growth and the onset of tumor-associated osteolytic lesions in experimental models of breast cancer. PLoS One, 2012. 7(1): p. e29615. [PubMed: 22253746]
64. Kothapalli R, et al. , Functional characterization of selective exosite-binding inhibitors of matrix metalloproteinase-13 (MMP-13) - experimental validation in human breast and colon cancer. Biosci Biotechnol Biochem, 2016. 80(11): p. 2122–2131. [PubMed: 27362887]
65. Stawikowski MJ, Stawikowska R, and Fields GB, Collagenolytic Matrix Metalloproteinase Activities toward Peptomeric Triple-Helical Substrates. Biochemistry, 2015. 54(19): p. 3110–21. [PubMed: 25897652]

Statement of Significance:

Genetic and pharmacological approaches show that bone-stromal-derived MMP-13 catalytic activity is critical for osteoclastogenesis, bone destruction, and disease progression.

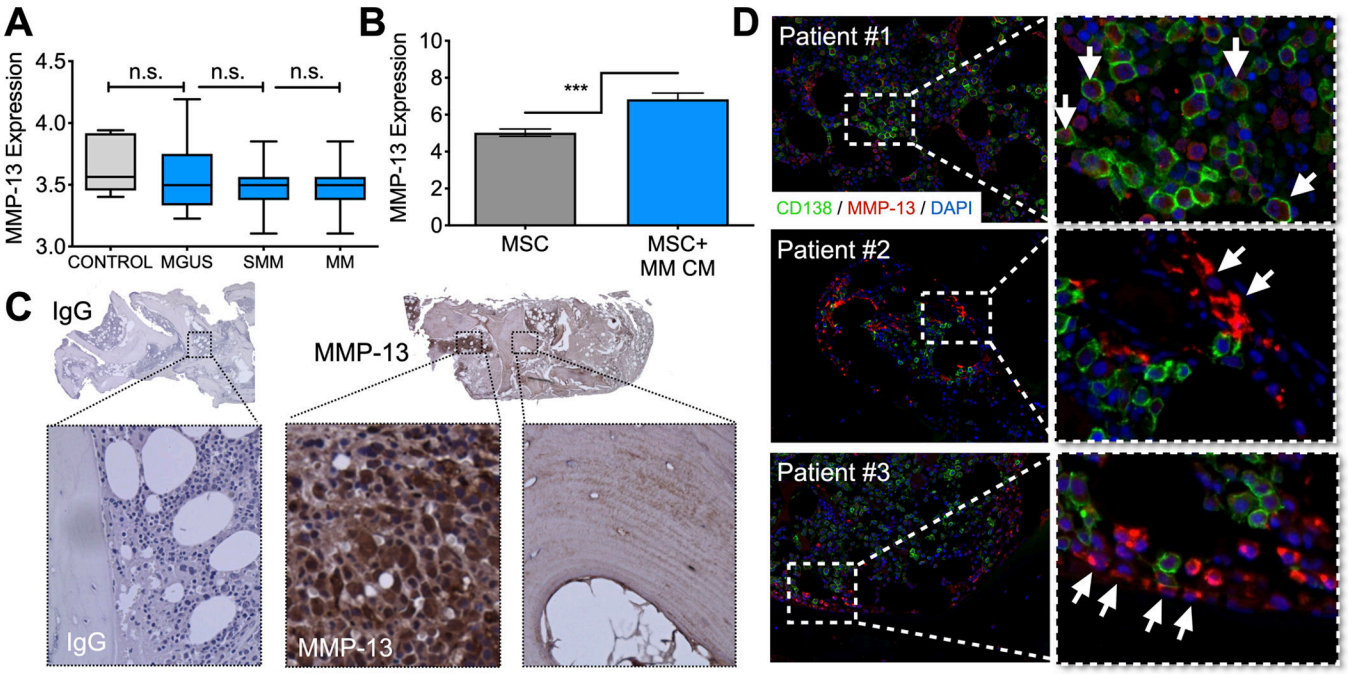

Figure 1.

MMP-13 is highly expressed by bone-lining mesenchymal stromal cells (MSC) in human multiple myeloma (MM). **A,** MMP-13 expression in CD138+ myeloma cells does not correlate with multiple myeloma disease staging. CD138+ myeloma cells isolated from human patients were analyzed for MMP-13 expression (GSE:47552; n=99 patients; n.s.). Control denotes healthy donor B cells. Monoclonal gammopathy of undetermined significance (MGUS) and smoldering multiple myeloma (SMM) represent progressive stages of multiple myeloma (MM). **B,** MMP-13 expression is enhanced in human MSCs exposed to multiple myeloma conditioned media. Publicly-available GEO transcriptomic dataset of human MSC treated with conditioned media from MM.1S human myeloma was analyzed (GSE:46053; n=37 samples; ***). **C,** MMP-13 is highly expressed in human multiple myeloma biopsies. Human multiple myeloma bone biopsies were immunohistochemically stained for MMP-13 and showed signal in marrow stroma and bone cement lines (Representative images shown from n=30 patients). **D,** MMP-13 is highly expressed by stromal cells at tumor-bone interface. Multiple myeloma patient bone marrow biopsies were immunofluorescently stained for MMP-13 (red). Myeloma cells were detected using CD138 (green) while nuclei were stained with DAPI (blue). Three representative patients (n=30 total). Dashed lines represent areas of magnification. Asterisks denotes statistical significance (***$p<0.0005$) while n.s. denotes non-significance.

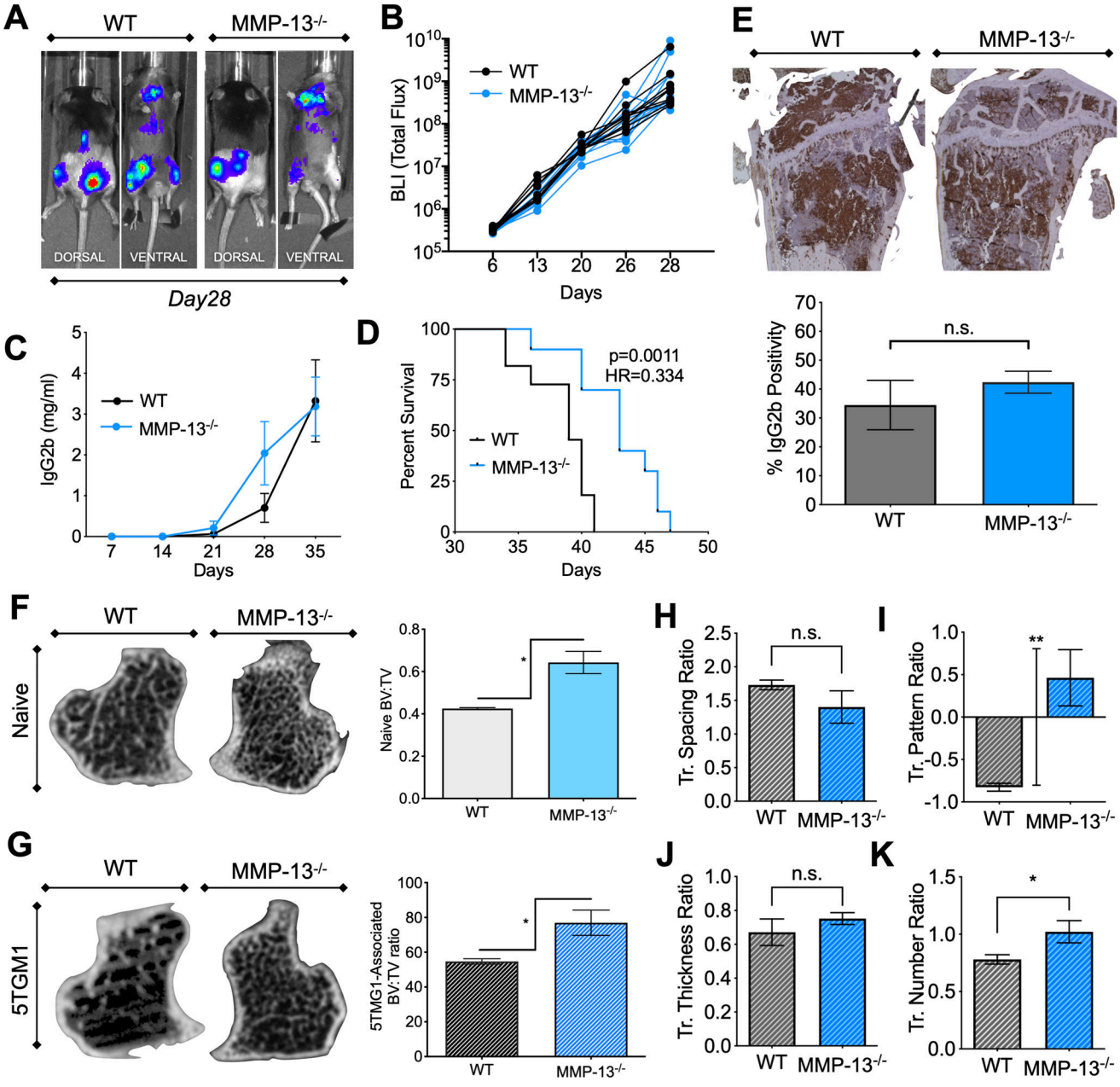

Figure 2.

Stromal MMP-13 ablation significantly reduces myeloma-induced osteolysis and improves overall survival *in vivo*. **A,** 5TGM1 myeloma colonizes skeleton of RAG2-null (WT) and RAG2/MMP-13-null (MMP-13$^{-/-}$) mice. Mice (n=20) were inoculated with luciferase-tagged 5TGM1 (10^6 cells/mouse) by tail-vein route to establish skeletal lesions. Mice were imaged once a week for bioluminescence. Representative images of skeletal tumor burden measurements 28 days after inoculation are shown. **B,** bioluminescence quantitation over time demonstrates no difference between the WT and MMP-13$^{-/-}$ groups. **C,** 5TGM1 cells secrete IgG2b antibodies, which was used as a surrogate for tumor burden. Serum IgG2b was measured by ELISA over time and corroborated bioluminescence data. **D,**

MMP-13-null myeloma bearing mice show improved overall survival. Mice were euthanized upon reaching clinical endpoint (greater than 10% weight loss or hindlimb paralysis). Kaplan-Meier curves were generated and statistically analyzed using log-rank test. Results show MMP-13$^{-/-}$ mice have significantly-delayed progression to clinical endpoint (median survival at 39 versus 43 days for WT and MMP-13$^{-/-}$, respectively). **E,** WT and MMP-13$^{-/-}$ mice have similar bone marrow tumor burden at study endpoint. Tibias were harvested from mice euthanized at endpoint for *ex vivo* analyses. Sections were stained for IgG2b by immunohistochemistry and showed extensive myeloma tumor burden across groups. Stained sections were quantified by area of IgG2b per total area of section (n=20; n.s.). **F,** tibias were harvested from 12-week old tumor-naive WT and MMP-13$^{-/-}$ mice for micro-computed tomography (μCT) scanning and quantitation to assess baseline bone status (BV:TV). Bones were scanned for 1000μm in the mid shaft at 6μm increments and contoured to highlight the bone marrow space (n=20). **G,** Tibia from multiple myeloma-bearing WT and MMP-13$^{-/-}$ mice were also collected at endpoint for same scanning and quantitation. Bone status from tumor-bearing tibias was normalized to tumor-naive data as BV:TV Ratio. **H-K,** Bone structure/patterning parameters were as measured via μCT. Asterisks denotes statistical significance (*p<0.05, **p<0.005) while n.s. denotes non-significance.

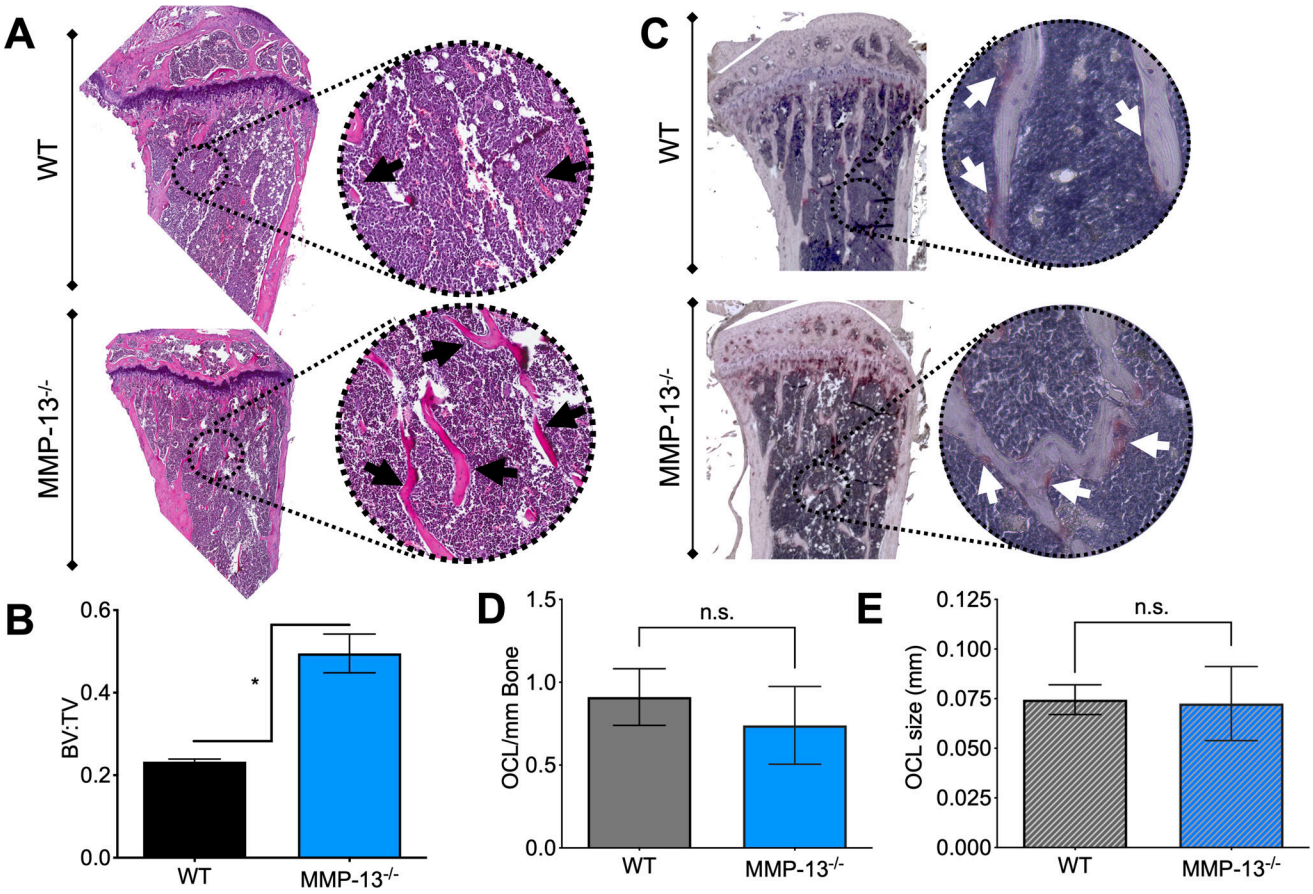

Figure 3.

Osteoclast size and number are not affected by host MMP-13 status in tumor-bearing tibias at disease endpoint. **A,** Tumor-bearing tibias were embedded in paraffin and sectioned at 5μm thickness for H&E staining (n=20). Staining allowed for visualization of trabecular bone and bone marrow compartments. **B,** H&E-stained sections were quantified for ratio of trabecular bone to total volume (BV:TV) and verified μCT findings (Student's t-test; *). **C,** sequential bone sections from each bone were stained for tartrate-resistant acid phosphatase (TRAcP) to visualize osteoclasts (red). Hematoxylin (blue) was used to identify cell nuclei. Representative images are shown. **D, E,** TRAcP-stained osteoclasts at the tumor bone interface were counted, their sizes measured and statistically analyzed by Student's t-test (n=20; n.s.). Asterisks denotes statistical significance (*$p<0.05$) while n.s. denotes non-significance.

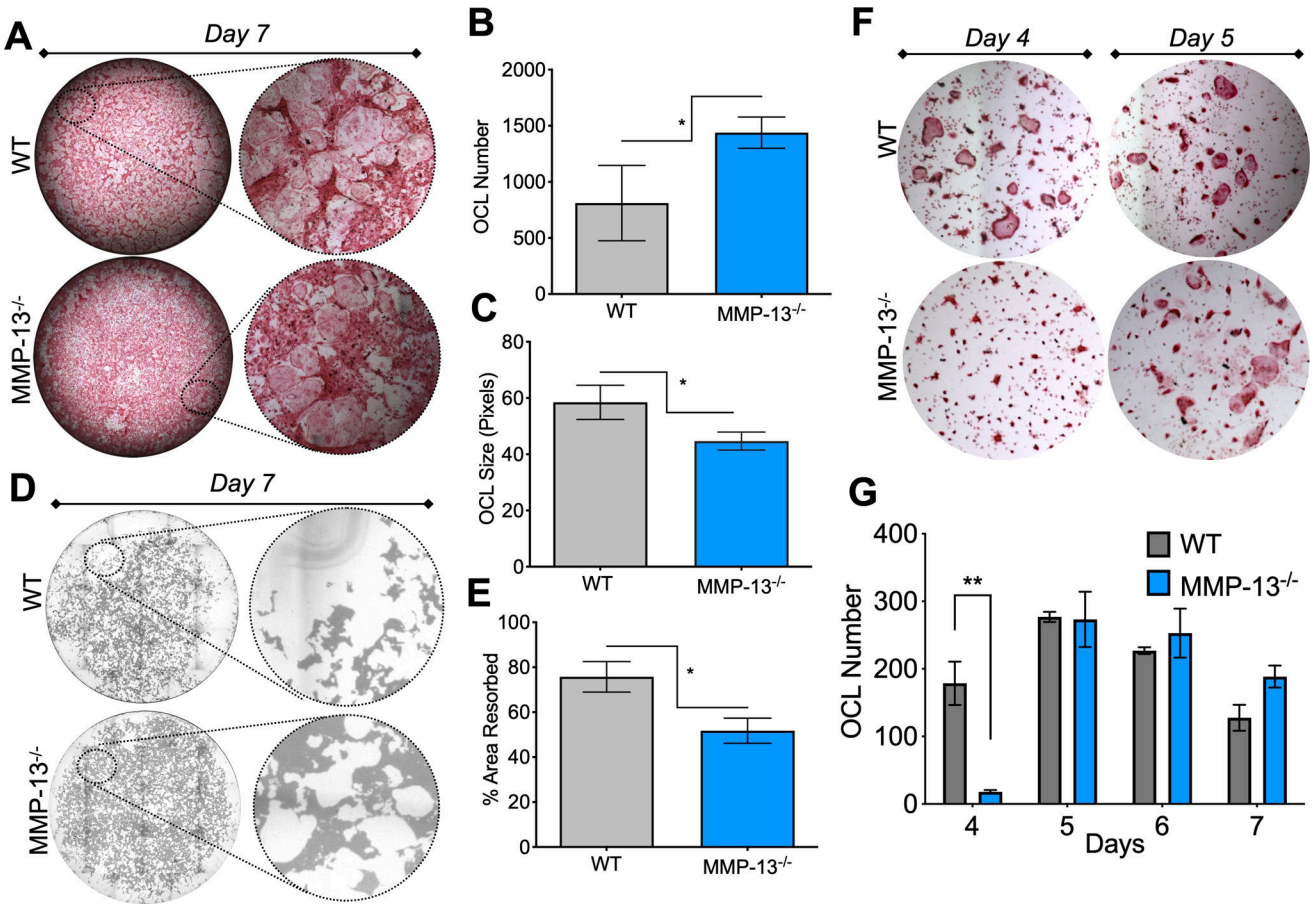

Figure 4.

MMP-13-ablation impacts osteoclastogenesis dynamics and resultant activity *in vitro*. **A,** Osteoclasts were differentiated using whole bone marrow co-cultures from 5–7-week old WT and MMP-13$^{-/-}$ mice. Co-cultures (20,000 cells/well in 96-well plate; n=3/group) were fed with fresh osteoclast media containing M-CSF and RANKL every other day for 7 days *in vitro* and fixed for TRAcP staining. **B, C** MMP-13$^{-/-}$ bone marrow co-culture generated more but smaller osteoclasts than WT counterparts. TRAcP stained cultures were quantitated for number and size of multinucleated osteoclasts using ImageJ (*). **D,** Resorption assay was used to evaluate WT and MMP-13$^{-/-}$ osteoclast activity. Equal numbers of WT and MMP-13$^{-/-}$ precursor osteoclasts were plated onto bone-mimetic hydroxyapatite for differentiation and resorption. Osteoclasts were removed after 7 days the plate was imaged using bright-field microscopy to measure the area in which osteoclasts solubilized mineralized calcium (white). **E,** MMP-13$^{-/-}$ osteoclasts exhibit reduced activity compared to WT osteoclasts. The total cleared area of resorption versus residual hydroxyapatite-coated surface (dark grey) was quantitated (n=3/group; *). **F,** Osteoclast differentiation assay to assess temporal rate of differentiation (n=3/group/time point). Plates were fixed at days 4, 5, 6 and 7 of differentiation for TRAcP staining and quantitation, representative images shown. **G,** Temporal quantitation analysis of multinucleate osteoclasts by WT and MMP-13$^{-/-}$ bone marrow reveal MMP-13$^{-/-}$ osteoclasts formed more slowly than WT osteoclasts (** at

day 4). Asterisks denotes statistical significance (*p<0.05, **p<0.005) while n.s. denotes non-significance.

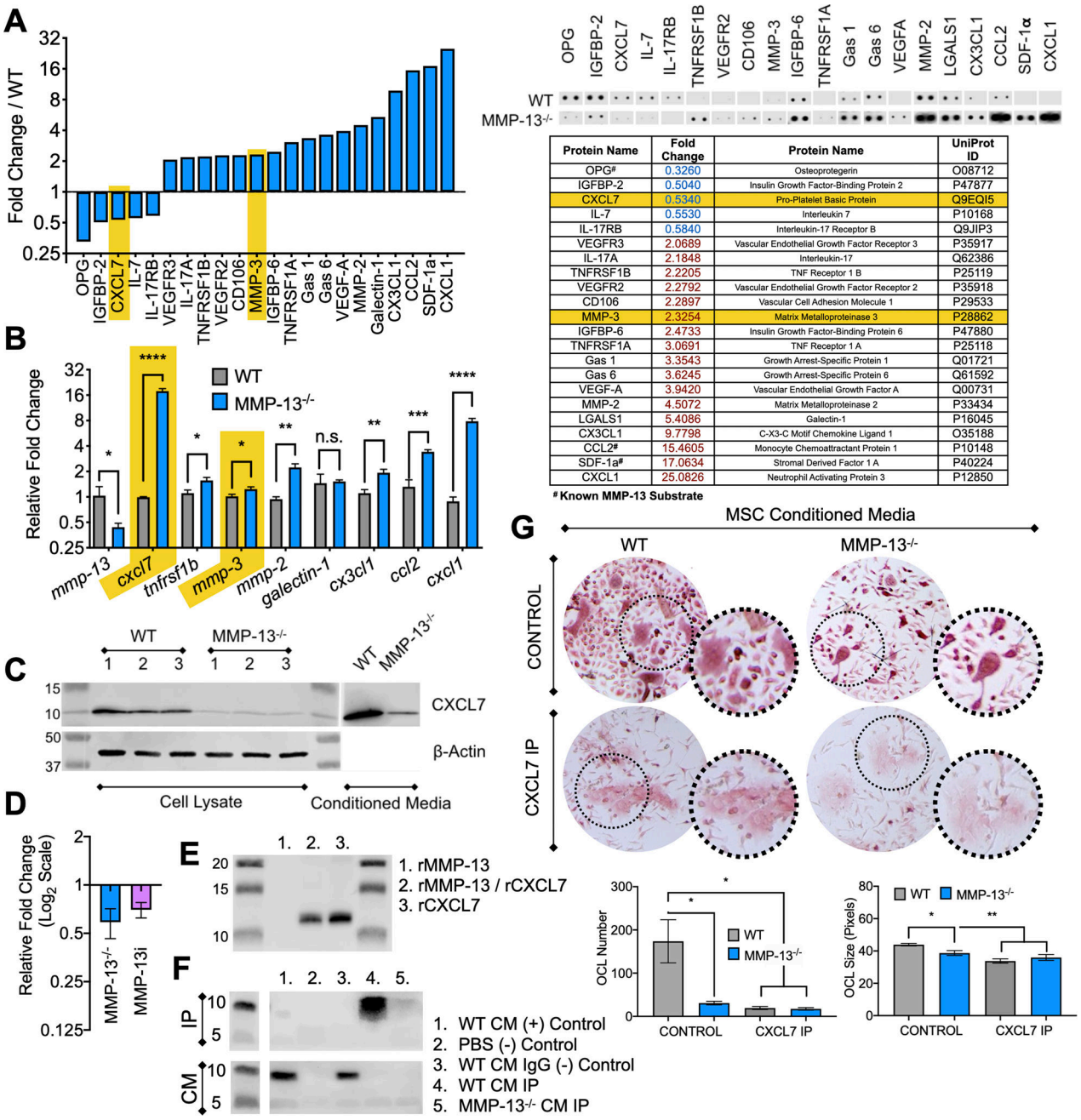

Protein Name	Fold Change	Protein Name	UniProt ID
OPG#	0.3260	Osteoprotegerin	O08712
IGFBP-2	0.5040	Insulin Growth Factor-Binding Protein 2	P47877
CXCL7	0.5340	Pro-Platelet Basic Protein	Q9EQI5
IL-7	0.5530	Interleukin 7	P10168
IL-17RB	0.5840	Interleukin-17 Receptor B	Q9JIP3
VEGFR3	2.0689	Vascular Endothelial Growth Factor Receptor 3	P35917
IL-17A	2.1848	Interleukin-17	Q62386
TNFRSF1B	2.2205	TNF Receptor 1 B	P25119
VEGFR2	2.2792	Vascular Endothelial Growth Factor Receptor 2	P35918
CD106	2.2897	Vascular Cell Adhesion Molecule 1	P29533
MMP-3	2.3254	Matrix Metalloproteinase 3	P28862
IGFBP-6	2.4733	Insulin Growth Factor-Binding Protein 6	P47880
TNFRSF1A	3.0691	TNF Receptor 1 A	P25118
Gas 1	3.3543	Growth Arrest-Specific Protein 1	Q01721
Gas 6	3.6245	Growth Arrest-Specific Protein 6	Q61592
VEGF-A	3.9420	Vascular Endothelial Growth Factor A	Q00731
MMP-2	4.5072	Matrix Metalloproteinase 2	P33434
LGALS1	5.4086	Galectin-1	P16045
CX3CL1	9.7798	C-X3-C Motif Chemokine Ligand 1	O35188
CCL2#	15.4605	Monocyte Chemoattractant Protein 1	P10148
SDF-1a#	17.0634	Stromal Derived Factor 1 A	P40224
CXCL1	25.0826	Neutrophil Activating Protein 3	P12850

Known MMP-13 Substrate

Figure 5.

Stromal MMP-13 differentially regulates the cytokine secretion profile of MSCs. **A,** MMP-13 impacts MSC secretion of cytokines. WT and MMP-13$^{-/-}$ MSCs were incubated in serum-free α-MEM for 24 hours to generate conditioned media (CM) that was then subjected to cytokine array analysis. Cytokines with greatest changes and known roles in osteoclast biology were plotted and tabulated. **B,** MMP-13$^{-/-}$ MSCs have significantly higher levels of CXCL7 expression. RNA was isolated from WT and MMP-13$^{-/-}$ MSC for cDNA synthesis and quantitative PCR analysis. qPCR was performed for hits from cytokine array (ranging from * to ****). MMP-3 and CXCL7 are highlighted in **A**

and **B** to note that overexpression of MMP-3, an upstream activator of CXCL7, didn't sufficiently rescue CXCL7 levels in MMP-13$^{-/-}$ MSCs. **C,** CXCL7 protein is downregulated in MMP-13$^{-/-}$ MSC. CXCL7 western blot analysis was performed on MSC cell lysates and CM**. D,** CXCL7 protein levels were validated by ELISA in WT MSC treated with Compound 1, a highly selective MMP-13 inhibitor (MMP-13i). **E,** Human recombinant CXCL7 was incubated with human recombinant active MMP-13 overnight at 37°C and the impact on CXCL7 processing was assessed by western blot. **F,** CXCL7 was immunoprecipitated (IP) from WT and MMP-13$^{-/-}$ MSC CM. WT and MMP-13$^{-/-}$ MSC CM were incubated with anti-CXCL7 antibody and protein G sepharose beads overnight to precipitate CXCL7. Resultant CM was collected and corresponding beads washed for validation by western blot (top and bottom panel, respectively). **G,** CXCL7-depleted WT CM impairs osteoclastogenesis. Osteoclast differentiation assay was performed using WT bone marrow co-culture with WT, MMP-13$^{-/-}$, and CXCL7-depleted CM supplemented with RANKL. Wells were fixed at day 4 and quantitated for number and size of osteoclasts. Resulting quantitation was statistically analyzed by One-way Anova with post hoc multiple comparison analysis (Tukey test; * and **). Asterisks denotes statistical significance (*p<0.05, **p<0.005, ***p<0.0005, ****p<0.0001) while n.s. denotes non-significance.

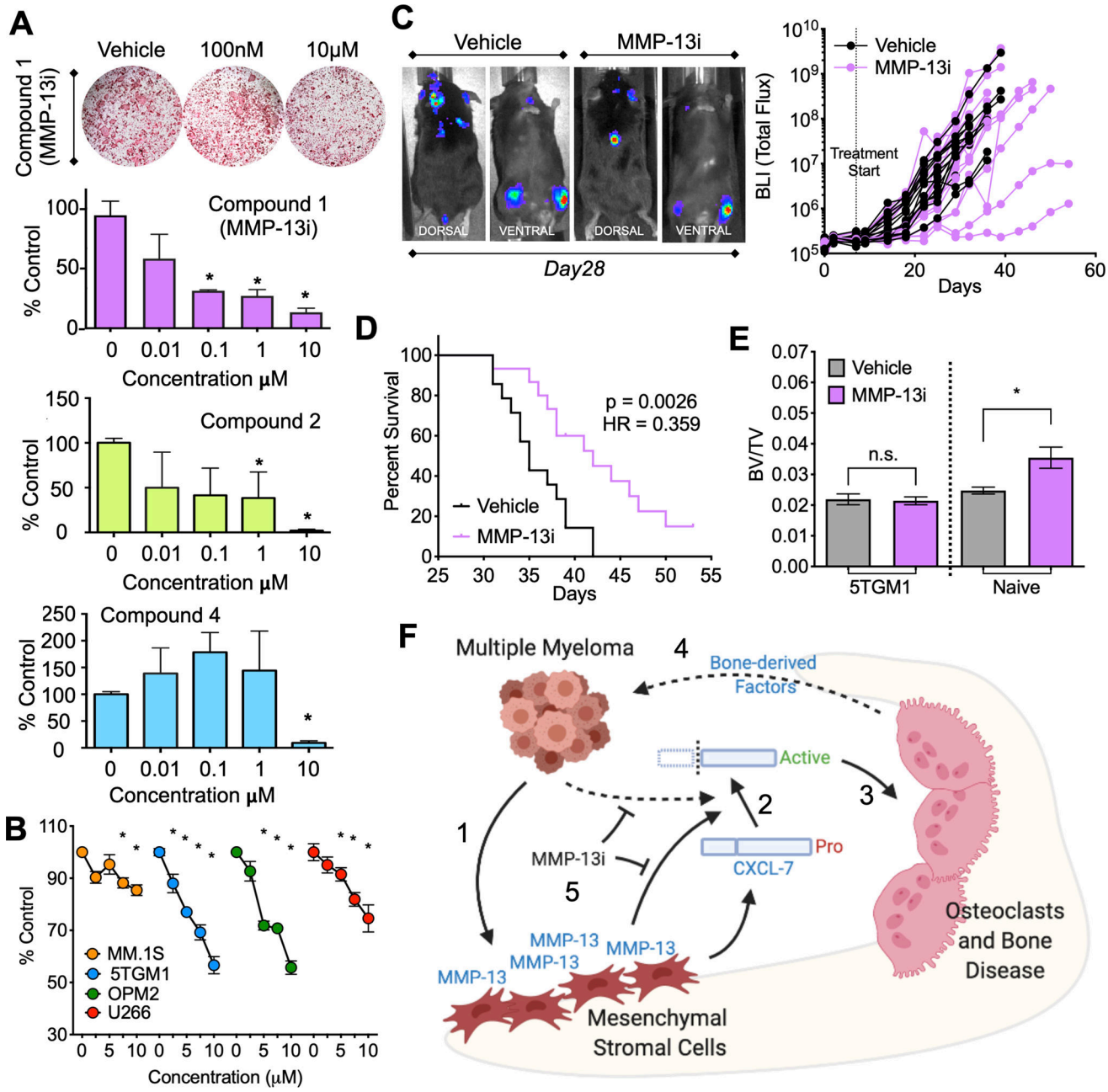

Figure 6.

Selective pharmacological inhibition of MMP-13 impacts multiple myeloma viability and osteoclast formation *in vitro*, and significantly improves overall survival *in vivo*. **A,** Osteoclast differentiation assays were performed in the presence of three MMP-13 inhibitors (n=3/concentration for each compound). Inhibitor compounds were administered every other day in fresh osteoclast differentiation media. Plates were fixed at day 7, TRAcP stained and quantitated for osteoclast numbers. One-way Anova statistical test was performed to assess osteoclast inhibition at each concentration of compounds compared to control group (*). **B,** Compound 1 (MMP-13i) strongly inhibited multiple myeloma viability. Multiple myeloma cell lines (MM.1S, 5TGM1, OPM2 and U266) were cultured in concentration

gradients of MMP-13i for 48 hours in 96-well plates (n=3/group). Cells were assessed by MTS and analyzed using a One-way Anova statistical test compared to the control group (*). **C,** MMP-13i treatment delayed multiple myeloma growth in immunocompetent syngeneic mouse model of multiple myeloma. luciferase-tagged 5TGM1 cells (n=10^6 cells/mouse) were inoculated into 5–6-week old syngeneic KaLwRiJ mice (n=30) by tail vein to establish skeletal lesions. Mice were randomly divided into Vehicle (10% DMSO 10% Tween80 in 1xPBS) and MMP-13i (20 mg/kg) group 7 days following tumor inoculation (n=15/group). Tumor growth was monitored by bioluminescence imaging and depicted as spider plot (BLI) twice a week until each mouse eventually reached endpoint hindlimb paralysis. **D,** Mice treated with MMP-13i demonstrated a significant increase in overall survival compared to vehicle control. Mice were euthanized upon reaching endpoints. Kaplan Meier curves were generated for each group (**; median survival: 35 vs 42 days for Vehicle and MMP-13i, respectively). **E,** Tibias harvested from control and MMP-13i MM-bearing mice (n=30) in addition to 7-week old control and MMP-13i treated tumor naïve groups (n=6/group) were subjected to μCT scanning and quantitation. MMP-13i treatment significantly increased bone volume in tumor-naive mice (Student's t-test: *). Tumor-bearing mice treated with MMP-13i removed from study at end-points mice showed similar bone volumes as analyzed by Student's t-test. Asterisks denotes statistical significance (*$p<0.05$ and **$p<0.005$) while n.s. denotes non-significance. **F,** Schematic of working model. 1. Multiple myeloma cells induce MMP-13 expression in MSCs. 2. MMP-13 can directly process CXCL7. 3. MMP-13 generated CXCL7 enhances osteoclast formation and activity. 4. Osteoclast mediated bone resorption generates further factors that promote myeloma cell survival and growth. 5. MMP-13 inhibition with highly selective inhibitors can block this myeloma and stromal derived MMP-13 to limit cancer associated bone disease and improve overall survival.